






Original Article


## Field investigations and numerical modeling of a giant landslide in the region of Eastern Himalayan Syntaxis: Jiaobunong landslide

**DU Guo-liang**<sup>1,2</sup>  <https://orcid.org/0000-0003-1081-9127>; e-mail: 756591925@qq.com

**ZHANG Yong-shuang**<sup>3\*</sup>  <https://orcid.org/0000-0002-8306-6464>;  e-mail: zhys100@hotmail.com

**YAO Xin**<sup>4</sup>  <https://orcid.org/0000-0003-3063-2546>; e-mail: yaoxinphd@163.com

**YANG Zhi-hua**<sup>4</sup>  <https://orcid.org/0000-0002-4372-3431>; e-mail: yangzh99@163.com

**YUAN Ying**<sup>1,2</sup>  <https://orcid.org/0000-0002-4985-4440>; e-mail: 275596117@qq.com

\*Corresponding author

<sup>1</sup> Hebei GEO University, Shijiazhuang 050031, China

<sup>2</sup> Key Laboratory of Intelligent Detection and Equipment for Underground Space of Beijing-Tianjin-Hebei Urban Agglomeration, Ministry of Natural Resources, Hebei GEO University, Shijiazhuang 050031, China

<sup>3</sup> Institute of Hydrogeology and Environmental Geology, Chinese Academy of Geological Sciences, Shijiazhuang 050061, China

<sup>4</sup> Institute of Geomechanics, Chinese Academy of Geological Sciences, Beijing 100081, China

**Citation:** Du GL, Zhang YS, Yao X, et al. (2021) Field investigations and numerical modeling of a giant landslide in the region of Eastern Himalayan Syntaxis: Jiaobunong landslide. *Journal of Mountain Science* 18(12). <https://doi.org/10.1007/s11629-020-6617-y>

© Science Press, Institute of Mountain Hazards and Environment, CAS and Springer-Verlag GmbH Germany, part of Springer Nature 2021

**Abstract:** Eastern Himalayan Syntaxis (EHS) is a tectonically active region that undergoes continuous geomorphic changes. Large landslides are predominant in this region. A giant landslide called Jiaobunong landslide on the northwestern flank of the EHS were studied and simulated to investigate the formation mechanism, evolutionary process, and failure mechanism of the landslide, so that we could better understand the large complex ancient landslides in this region. Field investigation, geological background analyses, and numerical modeling were conducted to reveal the natural and seismic characteristics, as well as dynamic process of the landslide. The results show that the Jiaobunong landslide was the result of long-term geological and geomorphic evolution. Uplift, river incision, weathering, fault creep, glaciation, and earthquakes play key roles in the formation of landslides. Given the huge landslide volume, strong seismicity of the

study area, proximity to an active fault, and the need for extra forces to induce landsliding, the Jiaobunong landslide was triggered by a paleo-earthquake. Using numerical simulation based on the discrete element method, the slope dynamic response of the earthquake as well as the mass movement and accumulation process was reproduced. Simulation results showed that the landslide movement experienced four stages: initiation phase (0–5 s), acceleration phase (5–35 s), deceleration phase (35–95 s), and the compaction and self-stabilization stage (after 95 s). The rock mass was disintegrated and experienced strong collisions during the movement. The dammed lake gradually disappeared because of long-term river incision by the overtopping river water. These processes play a vital role in the evolution of landforms in the region of EHS.

**Keywords:** Eastern Himalayan syntaxis; Ancient landslide; Formation mechanism; Evolution process; Tibetan Plateau

**Received:** 08-Dec-2020

**Revised:** 31-Mar-2021

**Accepted:** 25-Jul-2021

## 1 Introduction

Landslides are defined as the downslope mass movement of rock, debris, or soil (Cruden 1991). They can be triggered by rainfall, snowmelt, earthquakes, unloading, freeze-thaw cycles, and human activities (Evans et al. 2001; Dortch et al. 2009; Zhou et al. 2016). In mountain terrains, especially tectonically active mountain ranges, landslides and particularly giant landslides are important erosion processes and form parts of the evolution of topographic relief, which permits rapid hillslope adjustment to hillslope base-level lowering (Pinto et al. 2008; Gallo and Lavé 2014). Most landslides are linked to the evolution of fluvial valleys (Korup and Montgomery 2008; Larsen and Montgomery 2012). Large landslides often surge into river valleys and form landslide dams by blocking the flow of rivers, thereby affecting the catchment morphology and the size of the drainage basin or the fluvial morphology (Korup 2010).

As one of the most tectonically active and fastest uplifting regions on Earth, the eastern Himalayan Syntaxis (EHS) is extremely prone to landslides (Du et al. 2017). One of the largest recorded landslides is the Yigong landslide ( $3 \times 10^8 \text{ m}^3$ ), which occurred on April 9, 2000, in Bomi County, southeastern Tibet. The landslide dammed the Yigong Zangpo River and formed a dammed lake, which threatened 4,000 inhabitants of the lake region (Shang et al. 2003). The dam failed 62 days later and caused great property losses downstream, including the destruction of highways, bridges, and communication facilities (Shang et al. 2003; Delaney and Evans 2015). The Sedongpu landslide-debris flows ( $3,500 \times 10^4 \text{ m}^3$ ) blocked the Yarlung Zangbo River, forming a barrier lake on October 17, 2018 (Liu et al. 2019). The Layue landslide ( $1,000 \times 10^4 \text{ m}^3$ ), which occurred on August 29, 1967, destroyed dozens of cars on the G318 National Highway (Kong et al. 2003). The Zelongnong landslide-debris flows, which were caused by the Motuo earthquake, buried Zhibai Village, caused 98 casualties and temporarily blocked the Yarlung Zangbo River in 1950 (Du et al. 2017). In addition, numerous giant ancient landslides, such as the Wenlang and Jiazong landslides, occurred in the study area (Fig. 1). Because of the narrow valleys, deep incision, and high-steep hillslopes, these large landslides can easily block rivers. Understanding the formation mechanism and evolution of these large-scale landslides is crucial for designing preventive

measures for potential landslides as well as for the reconstruction of previous events and landscape evolution in the region of EHS.

However, restricted by natural conditions and poor transportation, landslides in this area have received little attention. The formation mechanism and evolution process of these landslides in EHS remain poorly understood. With high crustal uplift rate, high altitude and high earthquake intensity, the behaviors of landslides are nonlinear and very complex in the study area. At present, there are numerous methods to study the behaviors of landslides, including field survey and monitoring (Zhang et al. 2015; Guo et al. 2016; Doi et al. 2019), physical model experiments (Lin and Wang 2006; Song et al. 2018), and numerical simulations (Yin et al. 2012; Luo et al. 2012; Wang et al. 2020). Among them, numerical simulations are very effective and powerful tools for modeling the behavior of landslides and have been widely used. Numerical simulation methods mainly include continuum element methods and distinct element methods. Continuum methods, including finite difference method (FDM) and finite element method (FEM), are effective in modeling the slope stability under static and pseudo-static conditions; however, it is difficult to simulate the dynamic behavior during transport. Distinct element methods, which consider the effects of the discontinuities of a rock and can be used to analyze rock failure processes from micro-cracking to macro-cracking, are more efficient in determining the dynamic behavior of rock landslides. Thus, the distinct element methods are appropriate for the jointed rock slopes along deeply incised valleys in the EHS.

In this work, we studied a giant landslide called Jiaobunong landslide, which occurred on the northwestern flank of the EHS. The aim of this study was to investigate the formation mechanism, evolution, and failure mechanism of the Jiaobunong landslide. Remote sensing images, field geological surveys, and geological background analyses were used to determine the landslide boundaries, controlling factors, and formation mechanism of this giant landslide. To understand the evolution and failure mechanism of the landslide, the motion process of the landslide was reproduced using the discrete element method (DEM) with the Universal Distinct Element Code (UDEC) software. In addition, landslide trigger and the dam stability were discussed

based on field investigation and analysis. The results of this study provide key information about the origin and evolution of the Jiaobunong landslide.

## 2 Background

### 2.1 Regional geological setting

The study area is located in the eastern Himalayan syntaxis region of Tibet, China (Fig. 1). As a result of the collision between the Indian and Eurasian plates, the EHS region experienced rapid uplift, intensive tectonic compression, and deformation (Zhang et al. 2004; Xu et al. 2012) in combination with rapid incisions of rivers and glaciers. During this long process of geomorphic evolution, a typical alpine canyon region with an average elevation of >4 km was formed in the study area. Based on the deeply incised V-shaped valleys, the slopes experienced long-term unloading; the slope gradient on both sides of the rivers mainly ranges between 25° and 60°. Glacial landforms, which are mainly distributed in high mountains, were well developed. Based on historical earthquake records since 1331, more than 100 earthquakes occurred in the EHS region with magnitudes exceeding 4.7, including the

magnitude 7.7 southeastern Langxian earthquake in 1947 (Li et al. 2014), magnitude 8.6 Chayu earthquake in 1950 (Li et al. 2015), and magnitude 6.9 Linzhi earthquake in 2017.

The study area is characterized by a humid monsoon climate (Du et al. 2017). The warm-wet airflow of the Indian Ocean moves along the Yarlung Zangbo-Parlung Zangbo-Layue river canyon to the study area in the form of a “wet tongue” and is blocked by the Sejila Mountain; this airflow leads to rainfall in the study area. According to climate share data (1981-2010) from China Meteorological Data Service Centre (<http://data.cma.cn>), the annual precipitation in the Linzhi County ranges from 692 to 985 mm. The average annual temperature in the Linzhi County is ~9.1°C, while the maximum temperature is 31.4°C and the minimum temperature is -13.7°C. Overall, the climate is characterized by a large daily temperature difference, thin air, cold weather, and strong radiation, while significant changes have been observed in the vertical climate characteristics. Based on these climatic conditions, weathering (especially freezing weathering) at high slopes is extremely prevalent in the study area.

The EHS in Namcha Barwa is confined by faults (Zhang et al. 2004). The Milin Fault is a deformation belt at the western boundary of the EHS, which cuts

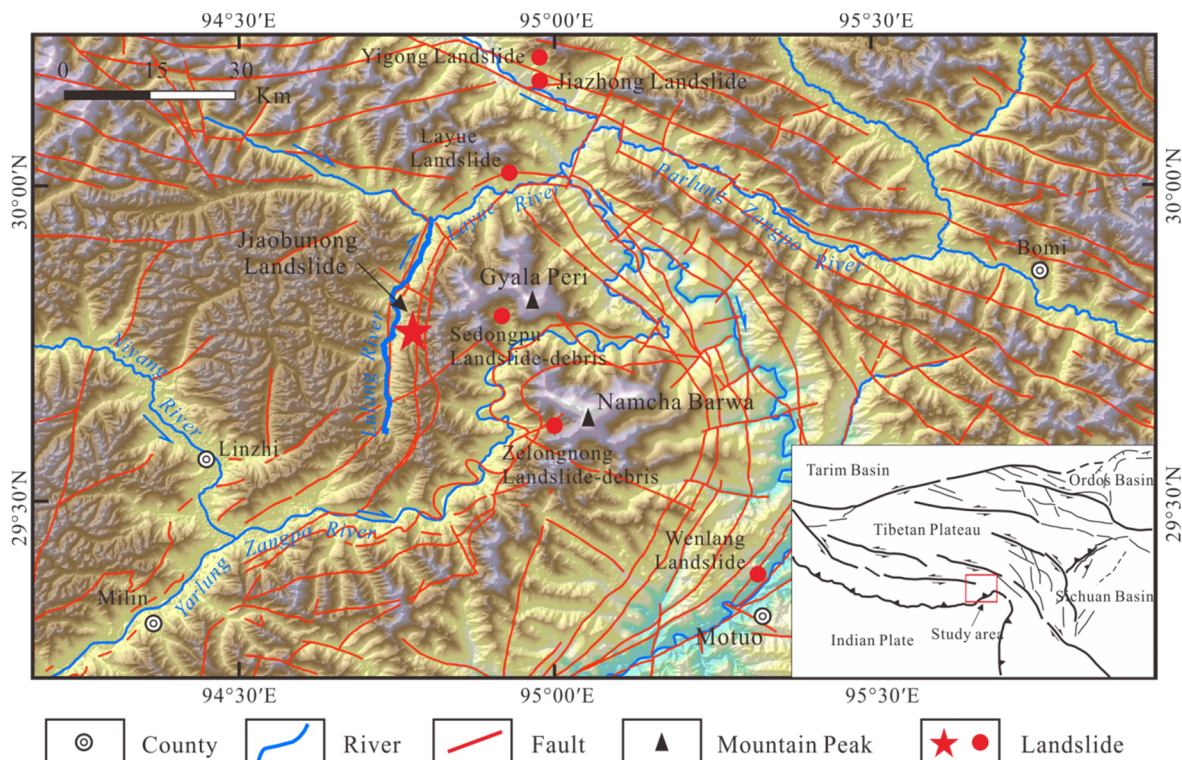


**Fig. 1** Map of the study area including large landslides.

through the Jiabunong landslide. From the Late Pleistocene to the Holocene, the Milin Fault has been very active; it exhibits a NE strike, SE dipping, and a dip angle of  $60^{\circ}$  to  $70^{\circ}$  (Zhang et al. 2004; Shao Cuiru et al. 2008). The Milin Fault extends from Milin County in the southwest to Tongmai Village in the northeast and controls the direction of the Parlung Zangbo and Lulang rivers. The rock masses near the fault zone are broken, and collapses and landslides occur frequently. These disasters resulted in the formation of natural barriers along the G318 National Highway including the famous Pailong natural barrier (Wang et al. 2013).

## 2.2 Basic characteristics of the Jiabunong landslide

### 2.2.1 Geographical and morphological characteristics

The Jiabunong landslide is located on the right bank of Lulang River near Zhongmai Village in Linzhi County, Tibet with the geographical coordinates of  $94^{\circ}45'23''$  E,  $29^{\circ}46'25''$  N. The Sichuan-Tibet Highway (G318 National Highway) passes through the landslide mass (Fig. 2).

The landslide crown, main scarp, left and right flanks, accumulation zone, and landslide toe can be easily identified (Fig. 3). The current geomorphic

feature of the landslide exhibits a tongue-like shape (Fig. 3), which is  $\sim 6.5$  km long and 1.6 km wide (Fig. 2). The main sliding direction of the landslide is  $\sim 290^{\circ}$ . The area of the accumulation zone is  $\sim 6.5$  km<sup>2</sup> and the average thickness of the sliding mass is  $>150$  m. Thus, the estimated volume of the landslide is  $>1000$  million m<sup>3</sup>. The head scarp of the landslide is above the snow line, whereas the toe of the landslide reaches the left bank of the Lulang River (Fig. 3). With a height difference of 1492 m between the head scarp and toe, the elevation ranges from 3344 to 4836 m (Fig. 4). Therefore, the angle of reach associated with the Jiabunong landslide is  $\sim 16^{\circ}$ , indicating the high mobility of the landslide.

The front of the original slope, which changed its course after the landslide, represented the accumulation area of the Jini Stream (Fig. 2). The landslide mass blocked the Lulang River and formed a dammed lake. Several landslide lakes developed on the accumulation body (Fig. 3). The front of the accumulation body was eroded and cut by the Lulang River. In the “V-shaped” valley, the cutting depth gradually increased from the upstream to the downstream, with a maximum depth of 270 m. The slope gradient of the dam along the Lulang River is  $\sim 40^{\circ}$ . The slopes are very unstable; certain slopes are currently undergoing creep deformation and some have already slipped down (Figs. 5a and b).

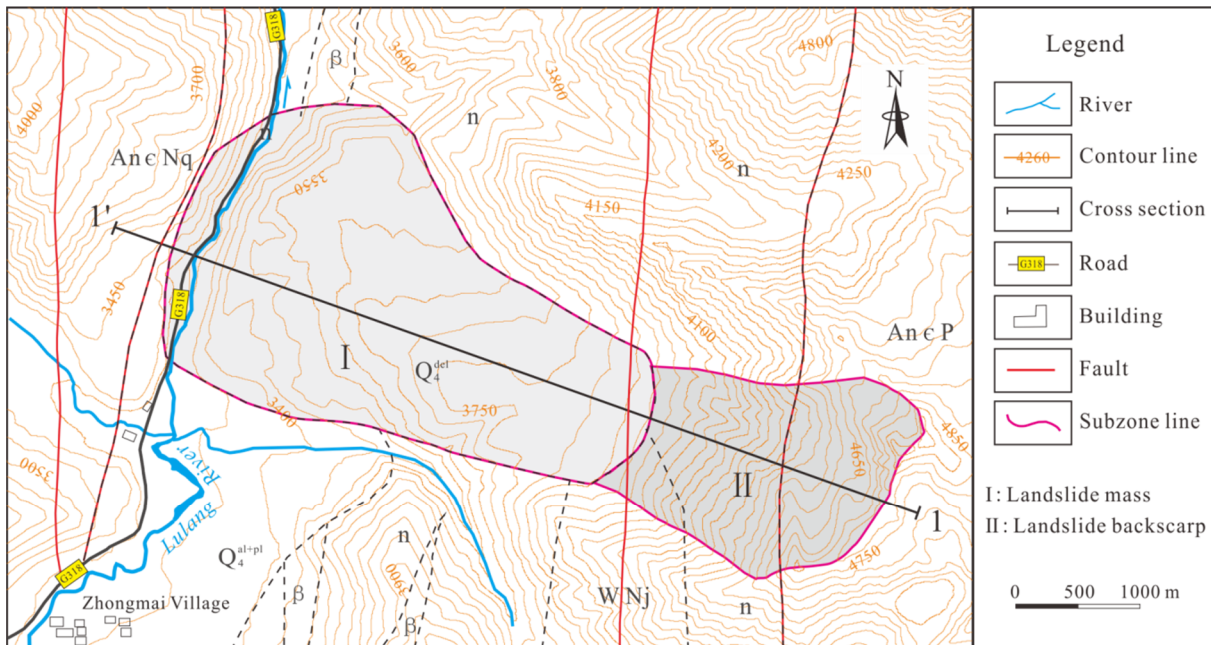


**Fig. 2** Engineering geological map of the Jiabunong landslide ( $Q_4^{al+pl}$ : alluvial - proluvial deposit; An  $\in$  P: Namjagbarwa Group Complex; An  $\in$  Nq: Nyenchen Tanglha Group Complex; n,  $\beta$ : ophiolitic mélangé belt rocks; WNj: exotic basement rocks.)

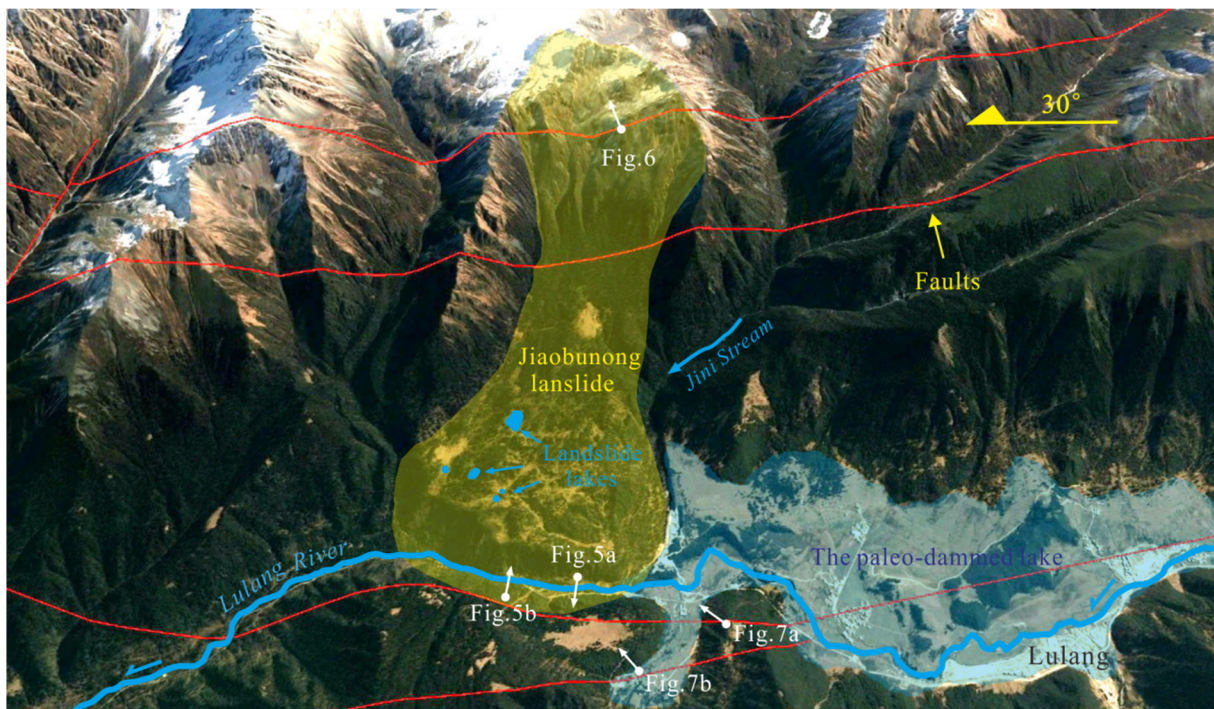


**Fig. 3** Remote-sensing image of the Jiaobunong landslide in Linzhi, Tibet, China.

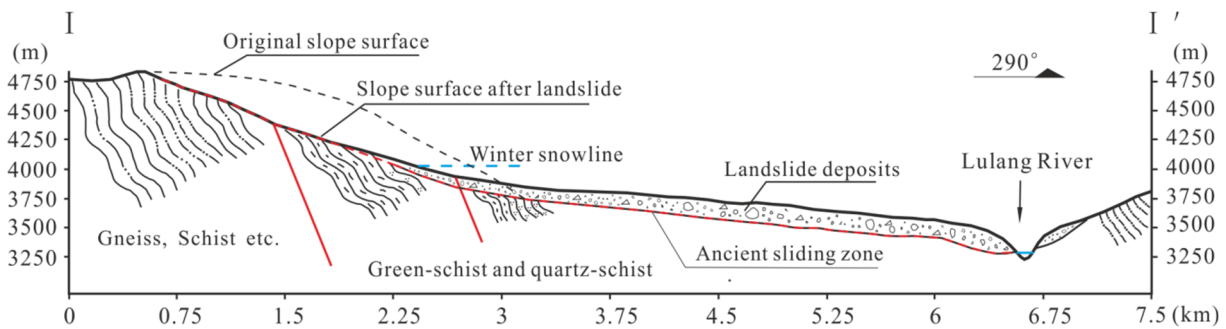


**Fig. 4** Cross-section of the Jiaobunong landslide.

### 2.2.2 Material and structure

Located in the Yarlung Zangbo suture zone, the regional strata mainly consist of the Nangarabawa Rock Group Complex (An & P), ophiolitic mélangé (n) and exotic basement rocks (WNj) (Fig. 2). The Nangarabawa Rock Group Complex primarily comprises gneiss and leptynite. The ophiolitic mélangé is predominantly composed of schist, green schist, and quartz schist. The exotic basement rocks are mainly made up of leptynite and marble. Owing to the cutting by the Milin Fault, strong weathering (seasonal and daily freeze–thaw cycles as well as rainfall), and frequent earthquakes, joints, cracks and deep fractures were developed and the slope rocks on the back and side walls were fragmented and loosened (Fig. 6). Based on Fig. 3, it can be concluded that

alluvial and fluvio-glacial deposits of Jini stream and Lulang River are primarily observed at the foot of the original slope (initial accumulation zone). After the sliding, the landslide accumulation area is mainly composed of fragmented stones, gravels, silts, and other debris, with diameters varying from several millimeters to tens of meters. The Lulang River cuts through the landslide deposits. Gravel and fine-grained alluvial deposits can be observed in the exposed profile on the right bank of the river on the dam. Several gullies developed on the backscarp of the landslide. Debris flows developed in the gullies and the debris was deposited on the landslide body.

### 2.2.3 Landslide barrier lake

After the slope failure, the landslide dammed the Lulang River and a barrier lake was formed. The

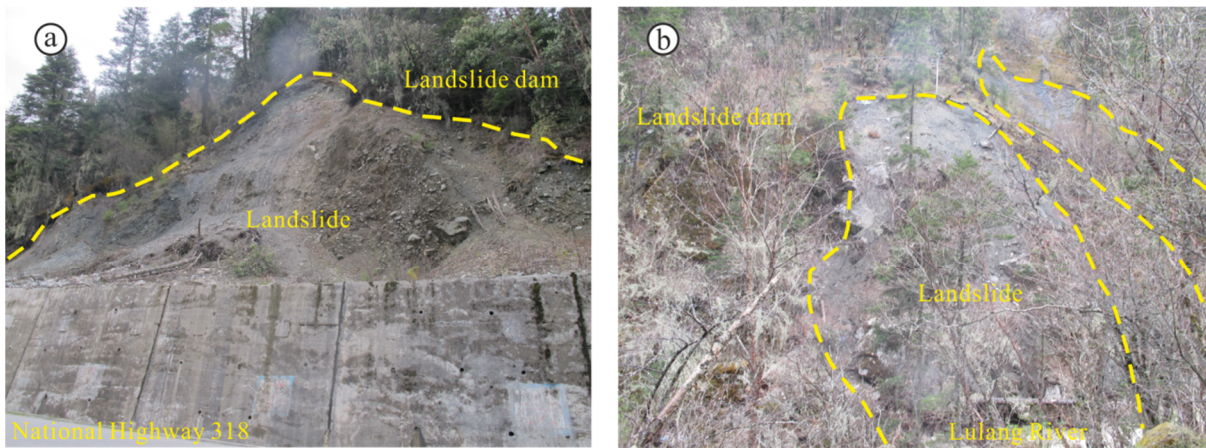


**Fig. 5** Secondary landslides on the landslide dam along the Lulang River: (a) Landslide on the left bank of the Lulang River (viewing direction: W) and (b) Landslide on the right bank of the Lulang River (viewing direction: direction E).

volume of the dammed lake was estimated as  $4.3 \times 10^9 \text{ m}^3$  approximately (Wang et al. 2019). Based on the study by Wang et al. (2019), the Jiaobunong landslide-dammed lake formed during the local Last Glacial Maximum (LLGM) before 24.2 ka cal. BP. Lacustrine sediments, which are composed of a succession of interbedded light yellow and light gray silty clay layers, can be found near Zhongmai Village (Fig. 7). The sedimentary layers are nearly horizontal, which reflects the stable hydrodynamic environment of the barrier lake (Fig. 7a). In the northern part, that is, near the southern foot of the landslide, the lake is shallow and gradually evolves toward the swamp. With the long-term erosion and dissolution of the dam, the barrier lake gradually disappeared after cutting off the landslide dam.

### 3 Formation Mechanism and Evolution Process of the Landslide

The rapid uplift of the region of the EHS and the rapid cutoff of the river in the past million years has resulted in the formation of alpine canyon landforms. Based on the endogenic and exogenic geological processes, many landslides have occurred in the study area, especially large-scale landslides. Numerous researchers have reported that the gestation of large-scale landslides in the study area is associated with the regional geological evolution (Shang et al. 2010; Zhou et al. 2016; Du et al. 2017). Based on the analysis of the regional geologic setting, geomorphologic evolution, and field investigations, the Jiaobunong landslide was a result of the coupling



**Fig. 6** Fragmented rock on the back scarp of the landslide (viewing direction: E).

of long-term geological evolution and short-term triggers. Its formation and evolution can be divided into the following four stages: initial deformation, cataclastic rock mass formation, earthquake-induced failure, and landslide damming and self-stabilization (Fig. 8).

#### 3.1 Initial deformation stage

Because of the movement of the Himalayas in the initial deformation stage, large-area crustal uplift and high valley incision occurred in the Lulang River. With the deepening of the river valley, the dominant local stress field gradually changed from tectonic to gravitational stress. Affected by unloading, the stress state of the slope rock notably changed. The top and foot of the slope area are characterized by tension and shear stress, respectively (Huang 2008). Under such

conditions, extension cracks formed in the rock at the top of the slope because of the unloading rebound deformation, while the rock at the foot of the slope underwent brittle deformation and shear cracks were formed.

### 3.2 Cataclastic rock mass formation stage

Because of the progressive failure of the earthquakes, creep of the Milin Fault, continuous

freeze–thaw cycles (seasonal and daily freeze–thaw cycles), loading–unloading cycle caused by the melting and freezing of glaciers in the glacial–interglacial cycle, and automatic expansion of water-filled fractures, the joints and cracks of the slopes expanded and some of them intersected with each other. Under the long-time action of the above-mentioned mechanisms, the rock mass was continuously cut and destroyed, resulting in the formation of cataclastic rock mass.

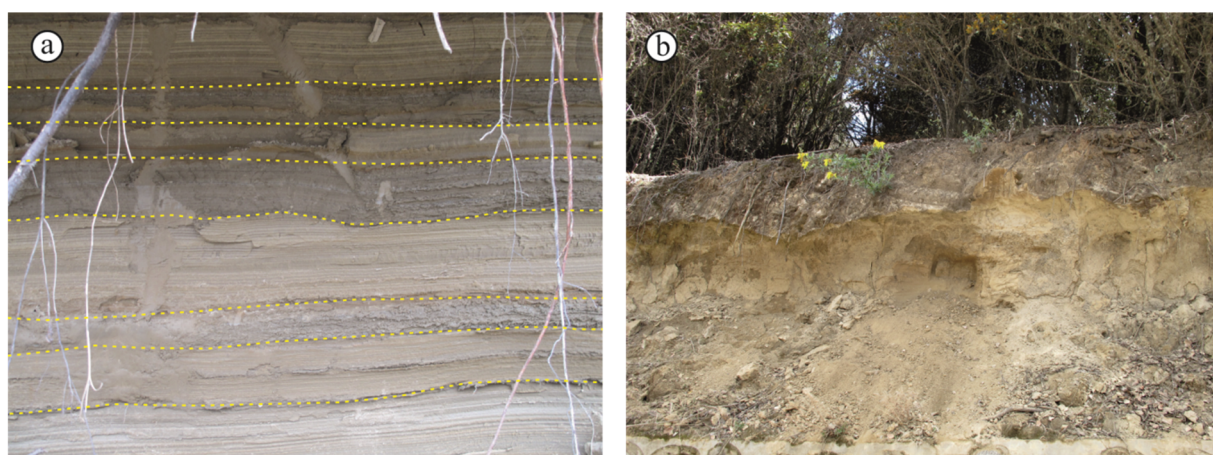


**Fig. 7** Lacustrine deposit of the dammed lake: (a) Lacustrine deposit on the left bank of the lake basin (viewing direction: SW) and (b) Lacustrine deposit on the terrace (viewing direction: EW).

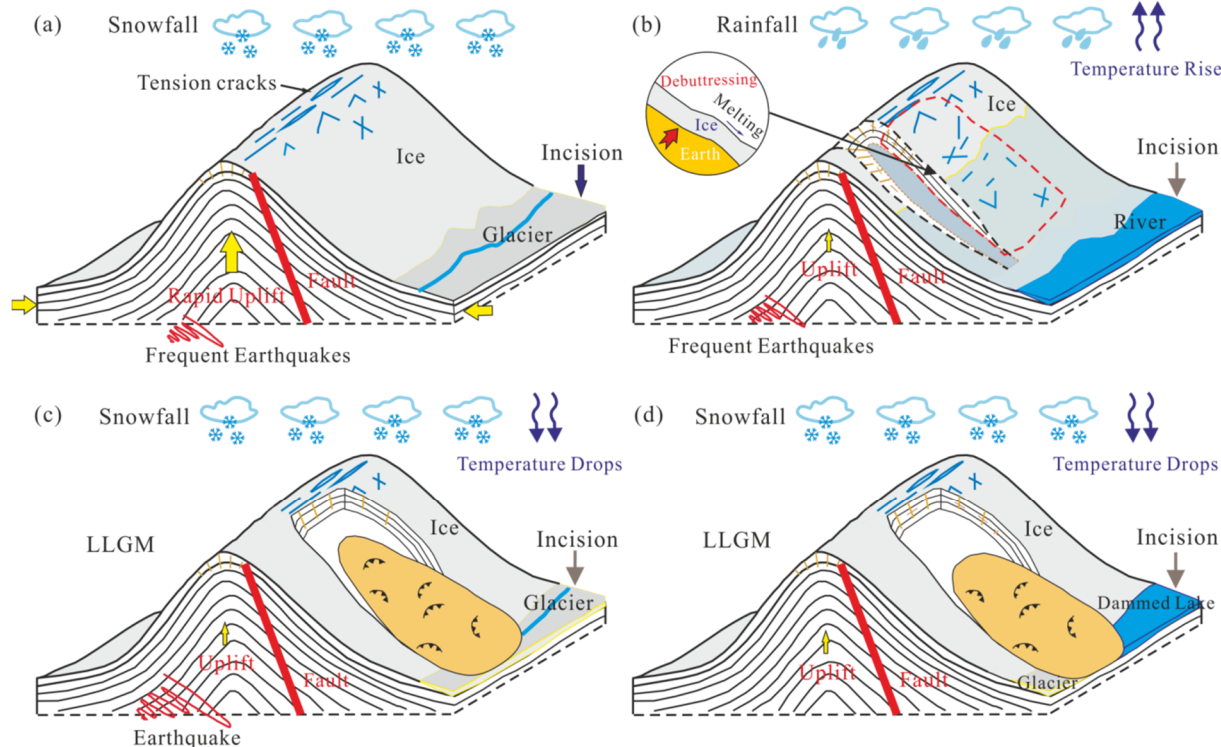


**Fig. 8** Evolution process of the Jiaobunong landslide: (a) Initial deformation stage, (b) Cataclastic rock mass formation stage, (c) Earthquake-induced failure stage, and (d) Landslide damming and self-stabilization.

### 3.3 Earthquake-induced failure stage

Under the action of seismic force (Du et al. 2017; Yang et al. 2020), the locked segment along the potential sliding surface of the slope body was sheared off. The gravity potential energy was released instantly and the slope body separated from the parent rock and moved down. During high-speed movement, the sliding blocks collided and the collision between the blocks and bedding led to rapid disintegration of the sliding body. During the movement, the sliding landslide mass carried and scraped the loose Quaternary sediments along the sliding direction, which resulted in an increase in the volume of the mass.

### 3.4 Landslide damming and self-stabilization

The landslide mass moved down the slope and blocked the Lulang River. The landslide mass stopped because of the resistance of the opposite slope; consequently, a landslide dam was formed. Because the dam was located upstream of the river, the flow of the Lulang River was small. The river water slowly accumulated and formed a semi-enclosed barrier lake. The dam was simultaneously compacted and self-stabilized by gravity. Because of the huge size of the dam and small river flow of the Lulang River, the landslide dam did not break quickly, but existed for a long time. Consequently, the water level of the lake increased; when it reached the crest position, water began to overflow from the dam. The water flow removed the dam material and a new discharge channel was formed. In combination with the constant incision, the barrier lake disappeared when

the level of the discharge channel reached the bottom of the lake. Meanwhile, the lake basin experienced slow deposition, which led to the formation of lake sediments.

## 4 Dynamic Analysis of the Long Run-out Slide Process

To reproduce and understand the evolution processes and failure mechanism of the Jiaobunong landslide under an earthquake, a dynamic analysis was carried out on the Jiaobunong landslide using the UDEC. The UDEC is a two-dimensional numerical simulation program based on the distinct element method. It can be used to simulate the response of a discontinuous medium under static or dynamic conditions (Itasca 1999). The UDEC can better reflect the characteristics of joints and faults of rock masses, allowing large displacement and rotation of blocks along discontinuities (Luo et al. 2012). The UDEC has been used to simulate the behaviors of several rock landslides (Bhasin and Kaynia 2004; Kveldevik et al. 2009; Luo et al. 2012; Pal et al. 2012; Zhou et al. 2013; Wang 2015).

### 4.1 Numerical model and parameters

Based on the topographic and geological cross-section taken along the main sliding direction (I-I' in Fig. 2), a simplified model of the Jiaobunong landslide was established, as shown in Fig. 9. The left and right boundaries of the model are 1.9 km and 800 m high, respectively; meanwhile, the bottom boundary is 7 km long. In the model, the bedrock and

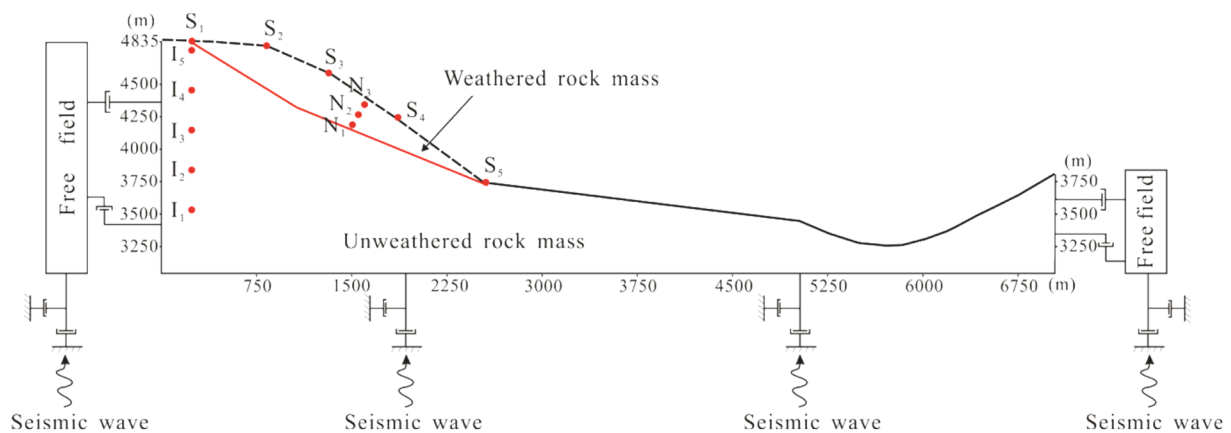


Fig. 9 Numerical calculation model for the Jiaobunong landslide.



**Table 1** Mechanical parameters of slope rock mass

Rock mass	Natural density (kg·m <sup>-3</sup> )	Cohesion (MPa)	Friction angle (°)	Bulk modulus (GPa)	Shear modulus (GPa)
Unweathered rock masses	2400	0.6	55	18.5	12.2
Weathered rock masses	2200	1.8	36	4.6	1.9

**Table 2** Mechanical parameters of structural plane

Structural plane	Normal stiffness (GPa·m <sup>-3</sup> )	Shear stiffness (GPa·m <sup>-3</sup> )	Cohesion (MPa)	Friction angle (°)
Bedding plane	25	21	0.05	20
Joint plane	25	21	0.04	15

landslide units consist of unweathered and weathered rock masses, respectively. The discontinuous surfaces are mainly joints and sliding surfaces.

The mechanical parameters of rock masses and joints are difficult to determine, and the simulated results tend to be influenced by the mechanical parameters (Zhou et al. 2013). Many empirical methods have developed to determine the mechanical parameters of a jointed rock mass (He et al. 2001; Singh and Rao 2005). Some scholars also study the effects of rock mass parameters on rock slope deformation (Du et al. 2006; Lv et al. 2012). In this study, the parameters of the rock masses and discontinuous surfaces are mainly based on the experimental parameters of the engineering rock mass grading standard and the empirical values used in previous successful simulations of similar landslides (Tables 1 and 2).

In addition, very high values of stiffnesses can prevent movement along a fictitious joint; however, the solution convergence tends to be very slow. Based on the UDEC manual (Itasca 1999), the normal stiffness ( $k_n$ ) and tangential stiffness ( $k_s$ ) of the joints should not exceed ten times the normal and tangential stiffness values of the hardest adjacent region:

$$k_n \text{ and } k_s \leq 10 \left[ \max \left[ \frac{K + 4G/3}{\Delta z_{\min}} \right] \right] \quad (1)$$

where  $K$  is the bulk modulus,  $G$  is the shear modulus, and  $\Delta z_{\min}$  is the smallest width of the zone next to the joint in the normal direction.

#### 4.2 Constitutive model and boundary conditions

In the model, the landslide rock masses adopt a plastic constitutive relation and the yield criterion is the Mohr–Coulomb failure criterion. The Coulomb slip model was used for the structural planes. In the static analysis, the horizontal displacement of the left

and right boundaries and the vertical displacement of the bottom boundary are fixed, such that the model reaches the equilibrium state under the self-weight condition. Under this condition, the dynamic analysis can be conducted. While performing the dynamic analysis, the static constraint at the bottom of the model was removed. The bottom of the model was set as the viscosity boundary and the left and right sides of the model were set as the free field boundaries (Zhang et al. 2016).

Despite the lack of records on paleoearthquake, it is important to analyze the behavior of the slope in an actual seismic environment. We note that El centro seismic wave, which is often used in dynamic response and dynamic failure mode of the slope studies (Ye et al. 2012; Cao et al. 2019; Zou et al. 2020), provides a realistic seismic input. The peak ground acceleration (PGA) distribution map with an exceeding probability of 2 percent in the future 50 years shows that the PGA in the study area is approximately 0.5–0.6 g. In this study, the adjusted horizontal El centro seismic acceleration wave (Fig. 10), which was adapted to the PGA, was obtained as the primary seismic wave. The vertical seismic acceleration was set to 2/3 of the adjusted natural horizontal seismic acceleration (Xu et al. 2012; GB 50011-2010. 2016).

The maximum frequency of the incoming seismic wave affects the maximum size of the model grid. Filtering the history and removing high frequency components is necessary (Itasca 1999). Based on the analysis of the Fourier spectrum, the main amplitude of the adopted natural seismic wave was  $\leq 5$  Hz. Thus, high-frequency components ( $>5$  Hz) of the original waveform were filtered out in this study.

During the dynamic analysis, the time history of the shear and normal stresses was applied at the bottom of the model with viscous boundary conditions. The time history of horizontal and vertical

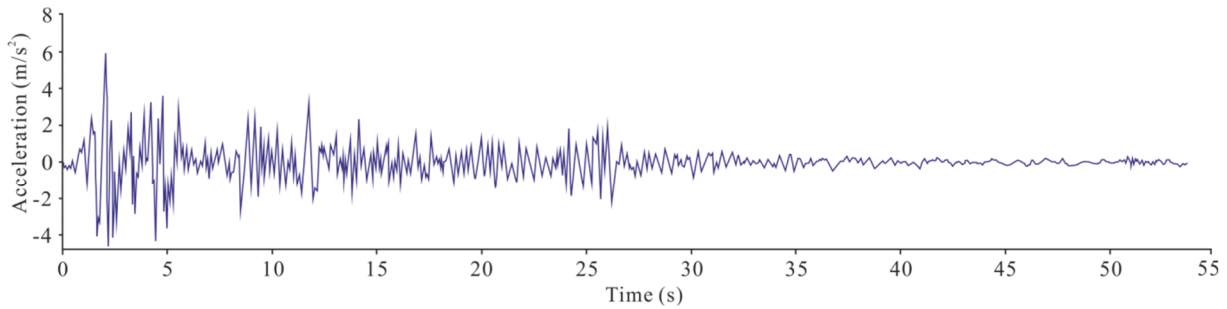


**Fig. 10** Acceleration time-history curve of the seismic-wave.

accelerations was first converted into velocity time history and then into stress time history by using the following equations (Pal et al. 2012; Zhou et al. 2013; Gao et al. 2021):

$$\sigma_s = -2(\rho C_s)v_s \quad (2)$$

$$\sigma_n = -2(\rho C_p)v_n \quad (3)$$

where  $\sigma_s$  and  $\sigma_n$  represent the shear stress and normal stress boundaries, respectively;  $\rho$  is the rock mass density;  $C_s$  and  $C_p$  are the velocities of the S- and P-waves, which can be calculated using Eq. (4) and Eq. (5), respectively; and  $v_s$  and  $v_n$  are the velocity components of the tangential and vertical vibrations, respectively.

$$C_s = \sqrt{\frac{G}{\rho}} \quad (4)$$

$$C_p = \sqrt{\frac{K + 4G/3}{\rho}} \quad (5)$$

### 4.3 Model grid size

To accurately simulate the propagation of the seismic waves and ground motion response during the dynamic analysis, the size of the model grid ( $\Delta l$ ) must be less than 1/10 to 1/8 of the wavelength of the seismic wave with maximum frequency:

$$\Delta l \leq a\lambda \quad a \in [1/10, 1/8] \quad (6)$$

where  $\lambda$  is the wavelength of the seismic wave with the maximum frequency, which can be obtained by the following equation:

$$\lambda = C_s / f_{\max} \quad (7)$$

where  $f_{\max}$  is the maximum frequency of the input wave.

The maximum frequency of the seismic input was 5 Hz, and the maximum grid size of the model was 45.08 m. To ensure the precision and accuracy in the calculation, computer memory, and computing speed

requirements, the model grid size was set to 40 m.

### 4.4 Analysis of the dynamic motion process

To analyze the dynamic response of the slope under the action of the earthquake, 13 monitoring points are chosen at different positions of the model to track the acceleration, velocity, and displacement of the slope varying with time. The locations of the monitoring points in the numerical model are shown in Fig. 9. Points S<sub>1</sub>, S<sub>2</sub>, S<sub>3</sub>, S<sub>4</sub>, and S<sub>5</sub> are on the slope surface; points I<sub>1</sub>, I<sub>2</sub>, I<sub>3</sub>, I<sub>4</sub>, I<sub>5</sub>, N<sub>1</sub>, N<sub>2</sub>, and N<sub>3</sub> are inside the slope; points S<sub>1</sub>, S<sub>2</sub>, S<sub>3</sub>, S<sub>4</sub>, S<sub>5</sub>, N<sub>1</sub>, N<sub>2</sub>, and N<sub>3</sub> are in the landslide mass; and points I<sub>1</sub>, I<sub>2</sub>, I<sub>3</sub>, I<sub>4</sub>, and I<sub>5</sub> are inside the landslide bed.

Fig. 11 presents the time history of the landslide mass displacement for different monitoring points. The displacements of the monitoring points show that the landslide stopped after ~95 s. As shown in Fig. 11a, the horizontal displacements of the monitoring points decrease with an increase in slope elevation. As shown in Fig. 11b, the vertical displacements of the monitoring points at the top of the landslide surface are larger than those of the lower ones. Point S<sub>2</sub> shows the largest vertical displacement as it is located on the steepest terrain. As shown in Figs. 11c and 11d, the horizontal and vertical displacements at the surface of the landslide are larger than those inside the landslide.

Fig. 12 presents the time history of the landslide mass velocity for different monitoring points. As shown in Fig. 12, the fluctuations of the horizontal and vertical velocities are significant, indicating strong collisions between the blocks. The collisions accelerated the disintegration of the landslide mass. As shown in Fig. 12a, the horizontal velocity of the rock masses at the foot of the landslide initially increased rapidly because of the lack of obstruction. Its maximum speed reached 72 m/s at ~60 s. Figs. 12b show that the vertical velocity is mostly negative,

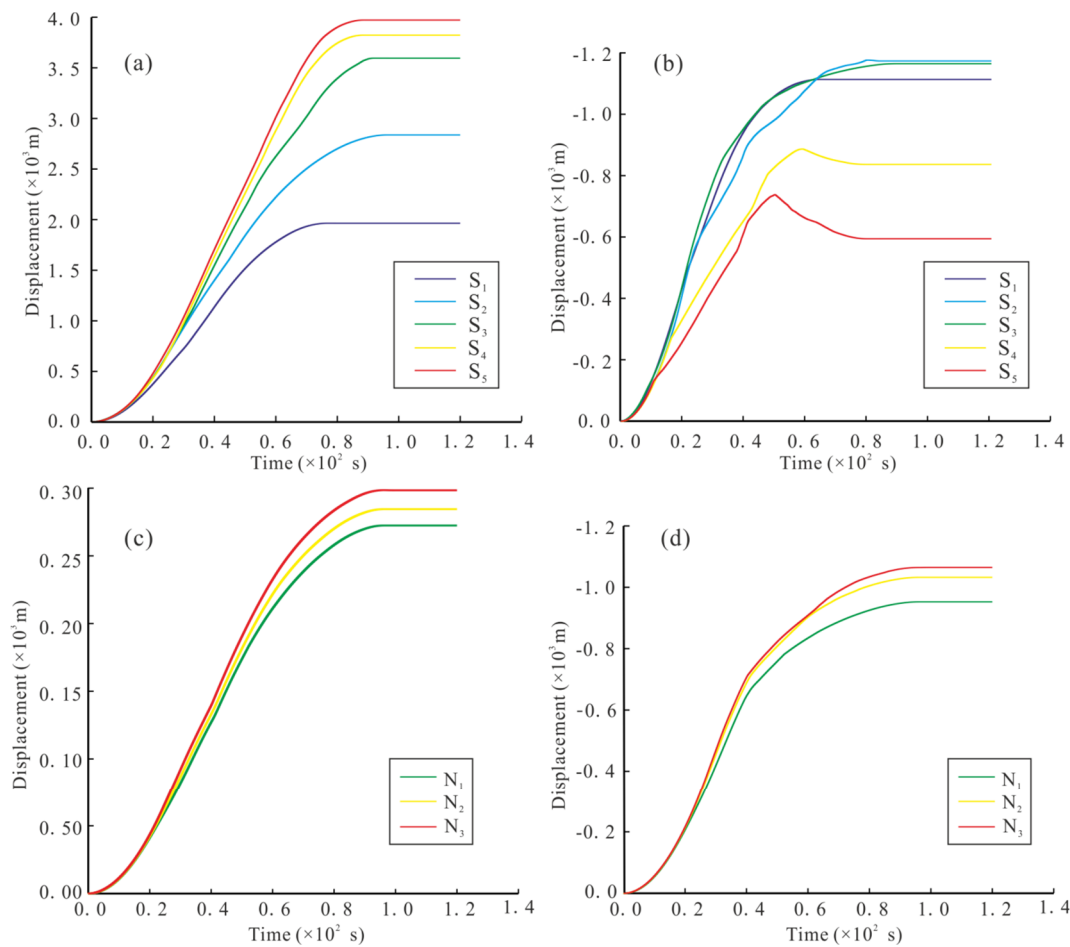


**Fig. 11** Time history of the monitoring point displacement of the slope: (a) and (b) are the horizontal displacement and vertical displacement on the slope surface, respectively, (c) and (d) are the horizontal displacement and vertical displacement of the landslide mass, respectively.

indicating that the landslide is moving downward. As shown in Figs. 12c and 12d, both the horizontal and vertical speeds inside the landslide mass are amplified, which indicates that the blocks at the surface generate less friction than that exhibited by the blocks present within the mass. The vertical velocities of the slope blocks on the surface fluctuated more than those of the blocks inside the slope (Fig. 12d); this result indicates that the blocks on the surface experienced vertical “jumping”, while they slid down because of the earthquake.

Fig. 13 presents the time history of the slope acceleration for different monitoring points. The horizontal and vertical PGAs tend to increase with elevation (Figs. 13a and 13b), thereby showing that maximum damage occurred at the top of the slope; subsequently, cracks were formed that initially extended at the top because of the earthquake. These results could also explain the formation of the top notch and the significant damage incurred by it

(Fig.6). The acceleration amplification leads to large horizontal and vertical tensile stresses at the top of the slope, providing favorable dynamic conditions for the formation of the top notch.

Fig. 14 presents the sliding process of the landslide. Affected by the earthquake, the slope became unstable and began to move along the sliding surface when the deformation of the slope reached a certain extent. As shown in Fig. 14, in the first 2 s of the seismic wave input, slope deformation is not notable. Subsequently, the seismic acceleration increased rapidly. After 5 s, the slope cracked and began to slide as a whole. Because of significant gravitational energy, the velocity of the shear outlet of the landslide increased rapidly. During the period of 5–35 s, the sliding body accelerated downward and parts of the landslide mass began to rush into the river. After 70 s, the river was completely blocked and parts of the landslide-debris rushed to the other side of the slope. Because of the resistance of the other

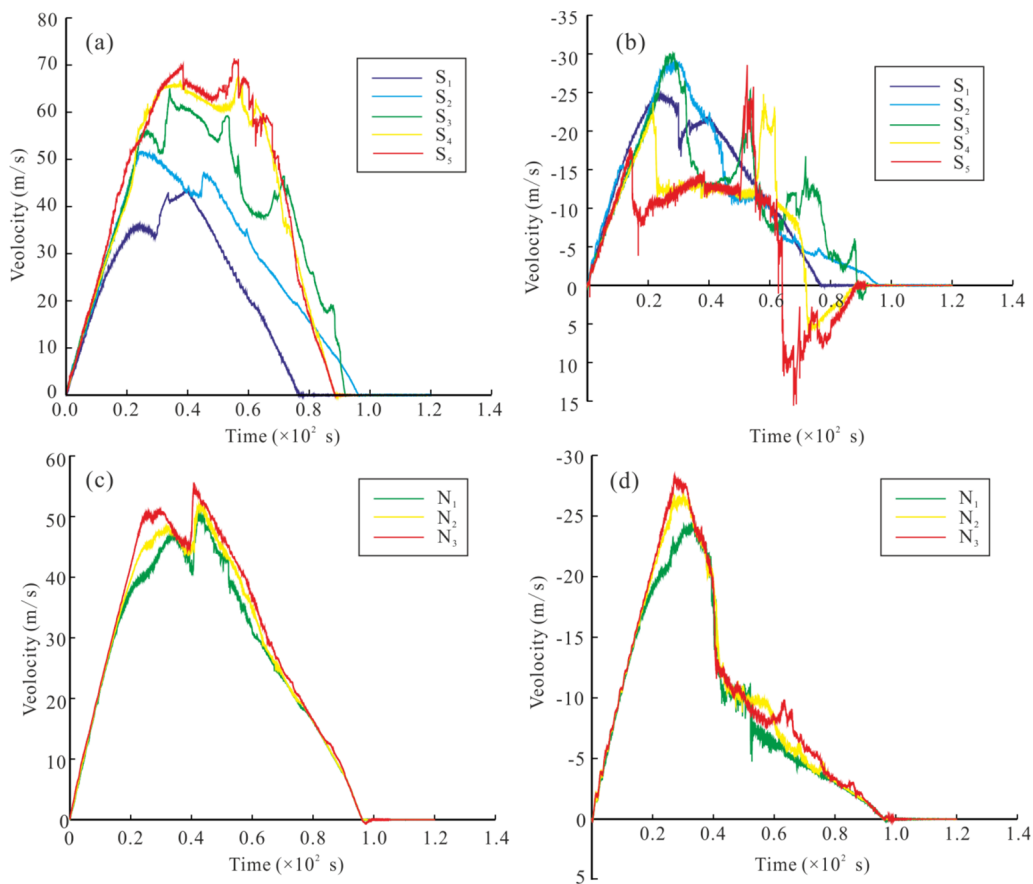


**Fig. 12** Time history of the monitoring point velocity of the slope: (a) and (b) are the horizontal velocity and vertical velocity on the slope surface, respectively, (c) and (d) are the horizontal velocity and vertical velocity of the landslide mass, respectively.

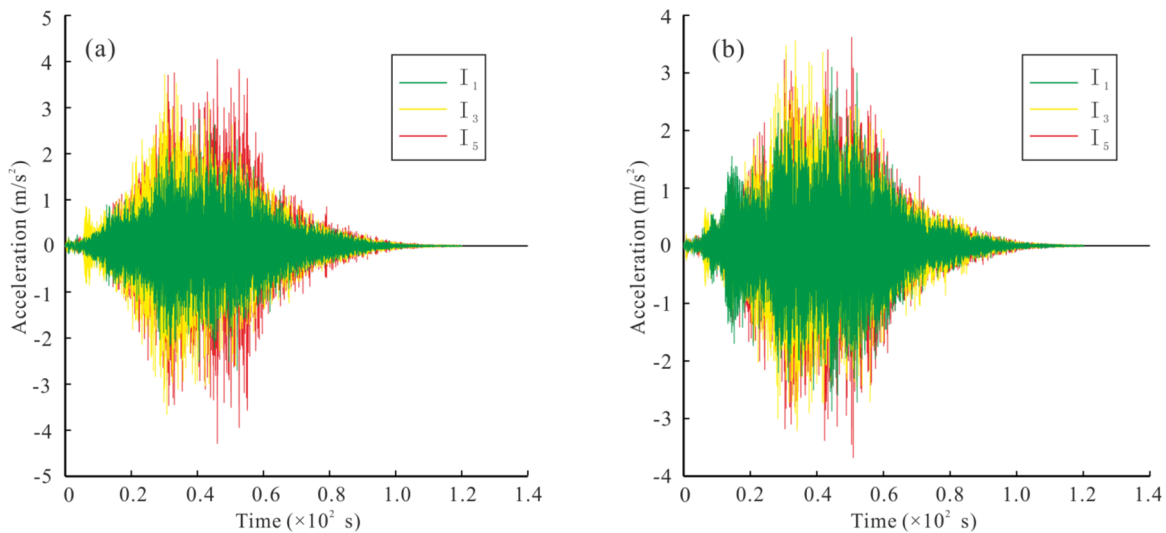


**Fig. 13** Time history of the monitoring point acceleration of the landslide mass: (a) horizontal acceleration and (b) vertical acceleration.

side of the slope, the movement stopped and a landslide dam was formed. After 95 s, compaction and self-stabilization of the landslide’s accumulation body

predominantly occurred under the action of gravity. Thus, the landslide motion can be divided into the following stages: initiation (0–5 s), acceleration (5–35

s), deceleration (35–95 s), and compaction and self-stabilization (after 95 s).

## 5 Discussion

### 5.1 Landslide trigger

It is well known that a high-position bedrock slope is extremely prone to damage under seismic action. Han (2015) identified indicators of large and giant bedrock landslides that were triggered by earthquakes in the Longmenshan tectonic belt of eastern Tibetan Plateau. Based on their results, it was observed that most large and giant bedrock landslides occur in regions with mean PGAs above 0.4 g. The lengths of the slip surfaces of the bedrock landslides triggered by earthquakes are larger than 100 m and

their depths are greater than 30 m. The relative difference in the elevations of potential landslides is larger than 200 m. The Jiaobunong landslide occurred in the EHS, which is characterized by strong tectonic activity and frequent occurrence of strong earthquakes. Tanay et al. (2015) analyzed GPS campaigns and seismic data in the region of EHS and concluded that the recurrence interval of earthquakes with magnitudes that exceed 8 is ~200 years. It is also well known that earthquakes with magnitudes above 4.0 can trigger landslides (Keefer 1984). The Jiaobunong landslide meets the characteristics of the large and giant seismic bedrock landslides that have been reported by Han (2015). The uneven slope surface at the top of the landslide is consistent with the surface shape formed by the ejection of the rock mass during the earthquake (Du et al. 2017; Yang et al. 2020). The huge landslide volume, strong seismicity

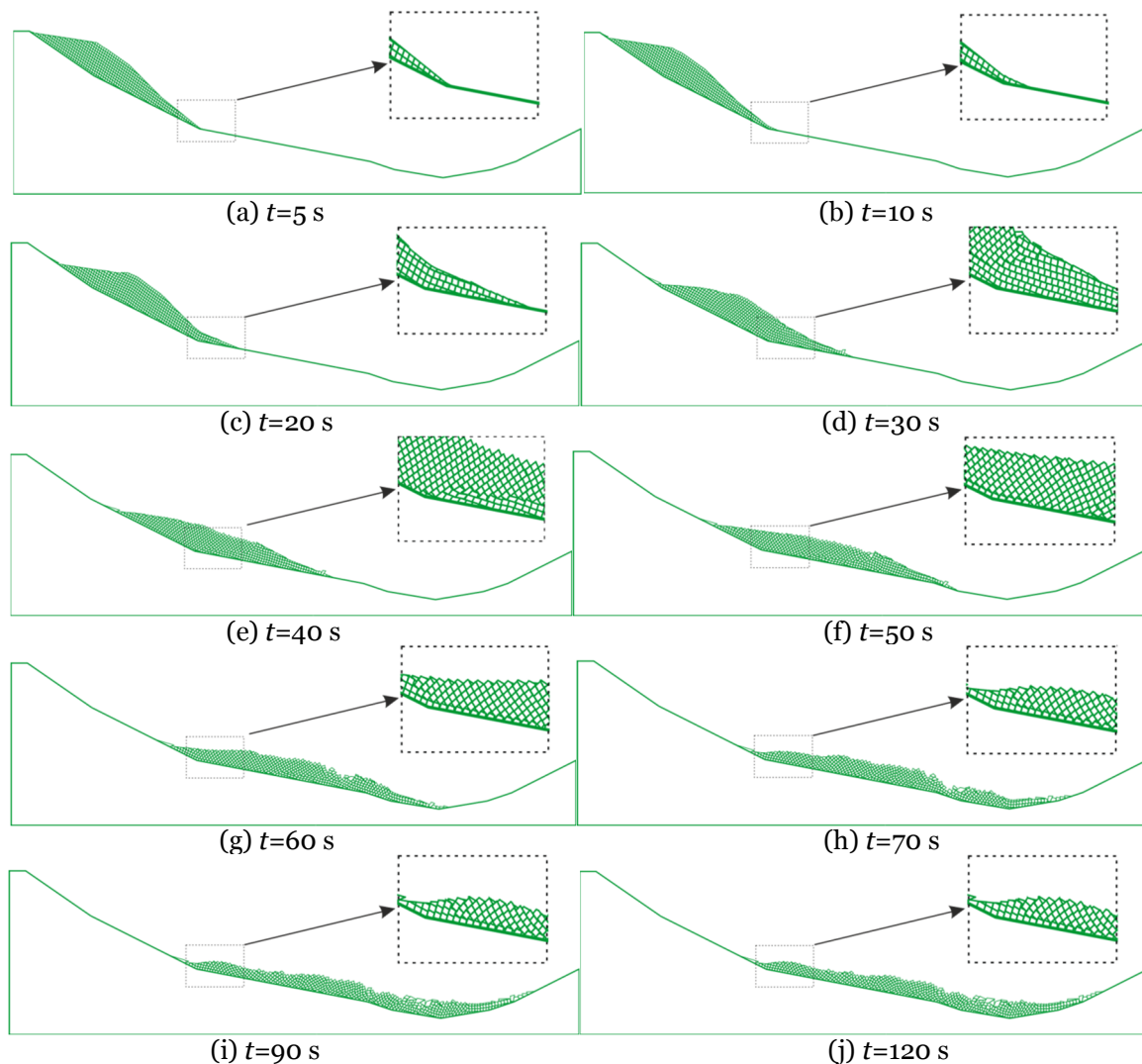


**Fig. 14** Jiaobunong landslide process according to seismic response.

of the study area, cutting by an active fault, and a need for additional forces to induce landslides suggest that the Jiaobunong landslide was triggered by an earthquake. The dammed lake was formed during the LLGM before 24 ka BP (Wang et al. 2019), while the LLGM at the region of the EHS occurred from ~30–13 ka BP (Hu et al. 2015). Considering the climate, precipitation, and glaciers cover during the LLGM, the influence of rainfall can be ignored. Furthermore, the onset of mountain glacier retreat occurred in Tibet at ~18–14 ka BP (Clark et al. 2009); thus, the landslide was not caused by glacial debuttressing. However, glacial debuttressing is a preparatory cause of the Jiaobunong landslide since it enables rock-slopes to destabilize more easily by seismic shaking.

## 5.2 Landslide runout distance

High velocity and long runout are important features of the Jiaobunong landslide. Evaluating the runout distance of a landslide is essential for hazard zoning and implementing disaster prevention and mitigation measures. The results of numerous studies showed that the angle of reach (H/L) decreases with increasing landslide volume (Scheidegger 1973; Corominas 1996). Several researchers also described a stronger correlation between landslide volume and runout distance (Legros 2002; Guo et al. 2016). However, the runout distance of the landslide is not only controlled by the volume and drop, but also by the topography of the sliding zone and its triggers. Fan et al. (2015) proposed a relationship between the volume ( $V$ ), slope height of drop ( $H_1$ ), slope gradient difference between the initiation zone and transporting zone ( $\alpha$ ), and horizontal moving distance ( $L$ ) of the landslide based on the data from 75 Wenchuan earthquake-induced landslides (>10000 m<sup>3</sup>). The equation is as follows:

$$L = 1.701V^{0.216} H_1^{0.510} (\tan \alpha)^{-0.107} \quad (8)$$

According to Fan et al. (2015), the multiple correlation coefficient of the model reaches 0.91, which exhibits an extremely high accuracy when predicting the horizontal moving distance of earthquake-induced landslides. We used Eq. (8) to predict the horizontal moving distance of the Jiaobunong landslide. Based on this equation, it was observed that the horizontal moving distance of the Jiaobunong landslide (~6.5 km) is close to the actual distance. This revealed that the Jiaobunong landslide

was induced by an earthquake.

In addition, glacial ice was well developed on the slope surface, while alluvial and fluvio-glacial deposits were well developed at the front of the initial landslide during the LLGM. It has been suggested that the presence of glacial ice on the slope and that of fluvio-glacial and alluvial deposits at the front of the slope reduce the friction of the landslide facilitate the long runout of the landslide. However, note that the landslide runout mobility is complex and depends on several factors including the topography, geomorphology, geologic material type and distribution, volume of the sliding mass, water content, strength parameters, and failure types (Guo et al. 2016; Zhu et al. 2019). Additional studies on the long runout should be conducted in the future, while considering the presence of glacial ice on the slope and the material composition of the Jiaobunong landslide movement channel.

## 5.3 Landslide dam stability

Landslide damming, which plays a vital role in the landform evolution in mountainous regions, is both composite and complex (Duman 2009). Landslide damming events are extremely hazardous and result in the expansion of geological hazards in the form of landslide chains (Du et al. 2017). Therefore, it is essential to evaluate the stability of a landslide dam for hazard mitigation and landscape evolution (Korup 2002).

Geomorphic approaches are widely used to correlate the dam, river, and impoundment characteristics with landslide-dam stability (Ermini and Casagli 2003; Dong et al. 2009, 2011). The landslide dam volume, dam height and dammed lake area are important factors that contribute to the stability of a landslide dam. Ermini and Casagli (2003) used the landslide dam volume ( $V_d$ ), dam height ( $H_d$ ) and catchment area ( $A_c$ ) to evaluate the stability of a landslide dam:

$$DBI = \log (H_d \cdot A_c / V_d) \quad (9)$$

If the dimensionless blockage index (DBI) is larger than 3.08, the dam is classified as unstable. If the DBI is smaller than 2.75, the dam is classified as stable. With these three variables, Dong et al. (2011) further developed an AHV\_Log model that uses the following calculation:

$$L_s = -4.48\log(A_c) - 9.31\log(H_d) + 6.61\log(V_d) + 6.39 \quad (10)$$

If  $L_s$  is greater than 0, the dam is regarded as a stable dam; otherwise, it is regarded as an unstable dam.

We used Eqs. (9) and (10) to predict the stability of the Jiaobunong landslide dam. The landslide dam is 1.7 km long, 2 km wide, and exhibits a volume of ~680 million m<sup>3</sup>. Meanwhile, the catchment area is approximately 5×10<sup>8</sup> m<sup>2</sup>. The DBI of the Jiaobunong landslide dam was determined as 2.17 (Fig. 15), while the  $L_s$  of the Jiaobunong landslide dam was 4.38; both these values indicate that the dam is stable.

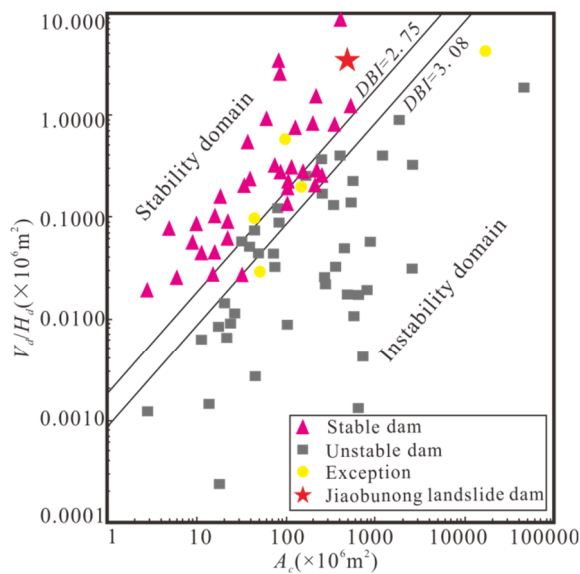


**Fig. 15** Result of the dimensionless blockage index (DBI) for Jiaobunong landslide dam (the other events are based on Ermini and Casagli (2003)).

In addition, in the upper reaches of the Lulang River, the flow of the river is small in the LLGM. The accumulation of Barrier Lake requires a certain amount of time, which provides the time for the compaction and self-stabilization of the huge landslide dam. Furthermore, the lacustrine sediments on the terrace show that the lake water overtopped the terrace and was deposited for a certain period (Fig. 7b). The horizontal lacustrine sedimentary layers reflect the stable hydrodynamic environment of the barrier lake (Fig. 7a). Based on the above-mentioned analysis, the landslide dam was stable overall and existed for a considerable period; however, it disappeared because a new channel was formed by the long-term incision of the overtopping lake water. After the disappearance of the lake, water erosion,

gravity, rainfall, and earthquake may contribute to the future occurrences of secondary landslides on the dam along the Lulang River, which threatens the Sichuan–Tibet Highway and might block the river again. Thus, detailed geotechnical investigations are recommended to evaluate the slope stability of the landslide dam along the Lulang River and predict the risk of future landslide damming.

## 6 Conclusions

In this study, various aspects of a typical, giant, ancient, and complex landslide (that is the Jiaobunong landslide) were investigated to determine the landslide features, formation mechanism and evolution process of the landslide. Based on field investigation and numerical modeling, the following conclusions have been drawn:

(1) The Jiaobunong landslide is a giant long-runout rock landslide with a volume >1000 million m<sup>3</sup>, a drop of 1492 m from 3344m to 4836m, a horizontal distance of ~6.5 km. The angle of reach is ~16°. According to the regional geologic and tectonic setting and field investigation, the Jiaobunong landslide was triggered by a paleo earthquake.

(2) The Jiaobunong landslide is the result of internal and external dynamic coupling, and it has experienced a long-term geological evolution. It formed under the combined action of crustal uplift, river incision, glaciation (loading–unloading cycle in the glacial–interglacial cycle), weathering (seasonal and daily freeze–thaw cycles), and tectonic movement (creep of the Milin Fault and frequent earthquakes), which resulted in the formation of favorable terrain, structural, and material conditions. The evolution of the Jiaobunong landslide can be divided into four stages: initial deformation, formation of cataclastic rock mass, earthquake-induced failure, and landslide blocking and self-stabilization.

(3) The instability of the landslide was reconstructed using numerical simulation based on the DEM. The simulation results show that the landslide stopped after ~95 s. The landslide movement was generally characterized by acceleration and deceleration. The speed at the foot of the landslide was larger than that at the top, while the speed in the shallow part of the slope was larger than that observed within the landslide. The movement of the landslide can be divided into four stages:

initiation, acceleration, deceleration, and self-stabilization.

(4) The Jiaobunong landslide blocked the Lulang River, which led to the formation of a dammed lake. Based on the field investigations and stability analysis, the landslide dam and the dammed lake were observed to be stable for a long time. However, the dammed lake disappeared after the formation of a new channel due to the long-term washing provided

by the overtopping river water.

## Acknowledgements

This study is supported by the Nation Natural Science Foundation of China (41941017, 41807231 and 41731287).

## References

- Bhasin R, Kaynia AM (2004) Static and dynamic simulation of a 700-m high rock slope in western Norway. *Eng Geol* 71(3-4): 213-226. [https://doi.org/10.1016/S0013-7952\(03\)00135-2](https://doi.org/10.1016/S0013-7952(03)00135-2)
- Cao L, Zhang J, Wang Z, et al. (2019) Dynamic response and dynamic failure mode of the slope subjected to earthquake and rainfall. *Landslides* 16(8): 1467-1482. <https://doi.org/10.1007/s10346-019-01179-7>
- Clark PU, Dyke AS, Shakun JD, et al. (2009) The last glacial maximum. *Science* 325(5941): 710-714. <https://doi.org/10.1126/science.1172873>
- Corominas J (1996) The angle of reach as a mobility index for small and large landslides. *Can Geotech J* 33(2):260-271. <https://doi.org/10.1139/t96-005>
- Cruden DM (1991) A simple definition of a landslide. *B Eng Geol Environ* 43(1): 27-29. <https://doi.org/10.1007/BF02590167>
- Delaney KB, Evans SG (2015) The 2000 Yigong landslide (Tibetan Plateau), rockslide-dammed lake and outburst flood: review, remote sensing analysis, and process modelling. *Geomorphology* 246: 377-393. <https://doi.org/10.1016/j.geomorph.2015.06.020>
- Dong JJ, Tung YH, Chen CC, et al. (2011) Logistic regression model for predicting the failure probability of a landslide dam. *Eng Geol* 117(1): 52-61. <https://doi.org/10.1016/j.enggeo.2010.10.004>
- Doi I, Kamai T, Azuma R, et al. (2019) A landslide induced by the 2016 Kumamoto Earthquake adjacent to tectonic displacement-Generation mechanism and long-term monitoring. *Eng Geol* 248: 80-88. <https://doi.org/10.1016/j.enggeo.2018.11.012>
- Dortch JM, Owen LA, Haneberg WC, et al. (2009) Nature and timing of large landslides in the Himalaya and Transhimalaya of northern India. *Quaternary Sci Rev* 28(11-12): 1037-1054. <https://doi.org/10.1016/j.quascirev.2008.05.002>
- Du G, Zhang Y, Yang Z, et al. (2017) Estimation of Seismic Landslide Hazard in the Eastern Himalayan Syntaxis Region of Tibetan Plateau. *Acta Geol Sin-Engl* 91(2): 658-668. <https://doi.org/10.1111/1755-6724.13124>
- Du TL, Zhang YX, Xie Q, et al. (2006) Effects of rock mass parameters on rock slope deformation. *Chin J Geol Hazard Control* 17(01):22-27 (In Chinese). <https://doi.org/10.3969/j.issn.1003-8035.2006.01.006>
- Duman TY (2009) The largest landslide dam in Turkey: Tortum landslide. *Eng Geol* 104(1): 66-79. <https://doi.org/10.1016/j.enggeo.2008.08.006>
- Ermini L, Casagli N (2003) Prediction of the behaviour of landslide dams using a geomorphological dimensionless index. *Earth Surf Proc Lan* 28(1): 31-47. <https://doi.org/10.1002/esp.424>
- Evans SG, Hungr O, Clague JJ, (2001) Dynamics of the 1984 rock avalanche and associated distal debris flow on Mount Cayley, British Columbia, Canada; implications for landslide hazard assessment on dissected volcanoes. *Eng Geol* 61(1): 29-51. [https://doi.org/10.1016/S0013-7952\(00\)00118-6](https://doi.org/10.1016/S0013-7952(00)00118-6)
- Fan XY, Leng XY, Duan XD (2015) Influence of topographical factors on movement distances of toe-type and turning-type landslides triggered by earthquake. *Rock Soil Mech* 36(5): 1380-1388. (In Chinese). <https://doi.org/10.16285/j.rsm.2015.05.021>
- Gallo F, Lavé J (2014) Evolution of a large landslide in the High Himalaya of central Nepal during the last half-century. *Geomorphology* 223: 20-32. <https://doi.org/10.1016/j.geomorph.2014.06.021>
- Gao G, Meguid MA, Chouinard LE, et al. (2021) Dynamic disintegration processes accompanying transport of an earthquake-induced landslide. *Landslides* 18(3): 909-933. <https://doi.org/10.1007/s10346-020-01508-1>
- GB 50011- 2010 (2016) Code for seismic design of buildings. China Archit & Build Press, Beijing.
- Guo CB, Zhang YS, Montgomery DR, et al. (2016) How unusual is the long-runout of the earthquake-triggered giant Luanshibao landslide, Tibetan Plateau, China? *Geomorphology* 259: 145-154. <https://doi.org/10.1016/j.geomorph.2016.02.013>
- Han JL (2015). The identification of large-giant bedrock landslides triggered by earthquake in the Longmenshan Tectonic Belt. *Acta Geol Sin-Engl* 89 (2): 681-682. <https://doi.org/10.1111/1755-6724.12460>
- He MC, Xue TH, Peng YF (2001) A new way of determining mechanical parameters of engineering rock masses. *Chin J Rock Mech Eng* 20(2): 225-229 (In Chinese). <https://doi.org/10.3321/j.issn:1000-6915.2001.02.017>
- Hu G, Yi CL, Zhang JF, et al. (2015) Luminescence dating of glacial deposits near the eastern Himalayan syntaxis using different grain-size fractions. *Quaternary Sci Rev* 124: 124-144. <https://doi.org/10.1016/j.quascirev.2015.07.018>
- Huang R (2008) Geodynamical process and stability control of high rock slope development. *Chinese J Rock Mech Eng* 27(8): 1525-1544. (In Chinese) <https://doi.org/10.3321/j.issn:1000-6915.2008.08.002>
- Keefer DK (1984) Landslides caused by earthquakes. *Geol Soc Am Bull* 95(4): 406-421. [https://doi.org/10.1130/0016-7606\(1984\)95&lt;406:LCBE&lt;2.0.CO;2](https://doi.org/10.1130/0016-7606(1984)95&lt;406:LCBE&lt;2.0.CO;2)
- Kong JM, Zhang XG, Qiang B (2003) Rock lump of landslide of layue destruction feature analysis in Sichuan-Xizhang Highway. *J Mt Sci* 21(2): 228-233 (In Chinese). <https://doi.org/10.3969/j.issn.1008-2786.2003.02.015>
- Korup O (2002) Recent research on landslide dams - a literature review with special attention to New Zealand. *Prog Phys Geogr* 26:206-235. <https://doi.org/10.1191/0309133302pp333ra>
- Korup O, Montgomery DR (2008) Tibetan plateau river incision inhibited by glacial stabilization of the Tsangpo gorge. *Nature* 455(7214): 786-789. <https://doi.org/10.1038/nature07322>
- Korup O, Montgomery DR, Hewitt K (2010) Glacier and landslide feedbacks to topographic relief in the Himalayan syntaxes. *P Natl Acad Sci* 107(12): 5317-5322.



- <https://doi.org/10.1073/pnas.0907531107>
- Kveldsvik V, Kaynia AM, Nadim F, et al. (2009) Dynamic distinct-element analysis of the 800 m high Aknes rock slope. *Int J Rock Mech Min* 46(4): 686-698. <https://doi.org/10.1016/j.ijrmmms.2008.10.007>
- Larsen IJ, Montgomery DR (2012) Landslide erosion coupled to tectonics and river incision. *Nat Geosci* 5(7): 468-473. <https://doi.org/10.1038/ngeo1479>
- Li BK, Diao GL, Zou LY, Xu XW, et al. (2014) The redetermination of the source parameters of the big earthquake M 7.7 in the southeast of Lang county in Tibet in 1947. *Seismol Geomagnetic Observ Re* 35(1): 85-91 (In Chinese). <https://doi.org/10.3969/j.issn.1003-3246.2014.01/02.017>
- Li BK, Diao GL, Xu XW, et al. (2015) Redetermination of the source parameters of the Zayü, Tibet M8.6 earthquake sequence in 1950. *Chin J Geophys* 58(11): 4254-4265 (In Chinese). <https://doi.org/10.6038/cjg20151130>
- Lin ML, Wang KL (2006) Seismic slope behavior in a large-scale shaking table model test. *Eng Geol* 86(2-3): 118-133. <https://doi.org/10.1016/j.enggeo.2006.02.011>
- Liu CZ, Lv JT, Tong LQ, et al. (2019) Research on glacial/rock fall-landslide-debris flows in Sedongpu basin along Yarlung Zangbo River in Tibet. *Geol China* 46(2): 219-234. (In Chinese). <https://doi.org/10.12029/gc20190201>
- Legros F (2002) The mobility of long-runout landslides. *Eng Geol* 63(3-4): 301-331. [https://doi.org/10.1016/S0013-7952\(01\)00090-4](https://doi.org/10.1016/S0013-7952(01)00090-4)
- Luo G, Hu X, Gu C, et al. (2012) Numerical simulations of kinetic formation mechanism of Tangjiashan landslide. *J Rock Mech Geotech* 4(2): 149-159. <https://doi.org/10.3724/SP.J.1235.2012.00149>
- Lv Q, Liu Y, Yang Q (2017) Stability analysis of earthquake-induced rock slope based on back analysis of shear strength parameters of rock mass. *Eng Geol* 228: 39-49. <https://doi.org/10.1016/j.enggeo.2017.07.007>
- Itasca (1999) Universal distinct element code user's manual. Itasca Consult Group Inc, Minneapolis.
- Pal S, Kaynia AM, Bhasin RK, et al. (2012) Earthquake stability analysis of rock slopes: a case study. *Rock Mech Rock Eng* 45(2): 205-215. <https://doi.org/10.1007/s00603-011-0145-6>
- Pinto L, Hérail G, Sepúlveda SA, et al. (2008) A Neogene giant landslide in Tarapacá, northern Chile: A signal of instability of the westernmost Altiplano and palaeoseismicity effects. *Geomorphology* 102(3-4): 532-541. <https://doi.org/10.1016/j.geomorph.2008.05.044>
- Scheidegger AE (1973) On the prediction of the reach and velocity of catastrophic landslides. *Rock Mech* 5(4): 231-236. <https://doi.org/10.1007/BF01301796>
- Shang Y, Yang Z, Li L, et al. (2003) A super-large landslide in Tibet in 2000: background, occurrence, disaster, and origin. *Geomorphology* 54(3): 225-243. [https://doi.org/10.1016/S0169-555X\(02\)00358-6](https://doi.org/10.1016/S0169-555X(02)00358-6)
- Shang Y, Yang Z, Yuan G, et al. (2010) Geohazards development and distribution along Sichuan-Tibet Highway in North of the Grand Canyon of Yarlu-Tsangpo. China Railway Publ House, Beijing. (In Chinese)
- Shao CR, You HC, Cao ZQ, et al. (2008) Tectonic Characteristics and Seismic Activities of Yaluzangbu Grand Canyon, Tibet, China. *Tech Earthq Disaster Preve* 12(4): 398-412. (In Chinese) <https://doi.org/10.1002/cne.902420109>
- Singh M, Rao K S. (2005) Empirical methods to estimate the strength of jointed rock masses. *Eng Geol* 77(1-2): 127-137. <https://doi.org/10.1016/j.enggeo.2004.09.001>
- Song D, Che A, Chen Z, et al. (2018) Seismic stability of a rock slope with discontinuities under rapid water drawdown and earthquakes in large-scale shaking table tests. *Eng Geol* 245: 153-168. <https://doi.org/10.1016/j.enggeo.2018.08.011>
- Tanay DG, Federica R, Sujit D, et al. (2015) Kinematics and strain rates of the Eastern Himalayan Syntaxis from new GPS campaigns in Northeast India. *Tectonophysics* 655: 15-26. <https://doi.org/10.1016/j.tecto.2015.04.017>
- Wang G (2015) Geoheritage features in Xi'an, China: Cuihua rock avalanche likely originating from an ancient earthquake. *Geoheritage* 7(3): 285-297. <https://doi.org/10.1007/s12371-014-0132-x>
- Wang H, Cui P, Liu D, et al. (2019) Evolution of a landslide-dammed lake on the southeastern Tibetan Plateau and its influence on river longitudinal profiles. *Geomorphology* 343: 15-32. <https://doi.org/10.1016/j.geomorph.2019.06.023>
- Wang PQ, Xu GT, He Q. (2013) Analysis on the causes of typical geological disasters in the southeastern Tibet and its prevention technology. *J Tibet Univ* 28(1):22-26 (In Chinese). <https://doi.org/10.16249/j.cnki.54-1034/c.2013.01.002>
- Wang H, Liu S, Xu W, et al. (2020) Numerical investigation on the sliding process and deposit feature of an earthquake-induced landslide: a case study. *Landslides* 17(11): 2671-2682. <https://doi.org/10.1007/s10346-020-01446-y>
- Xu WJ, Chen ZY, He BS, et al. (2010) Research on river-blocking mechanism of XiaojiaQiao landslide and disasters of chain effects. *Chin J Mech Eng* 29(5): 933-942 (In Chinese).
- Xu Z, Ji S, Cai Z, et al. (2012) Kinematics and dynamics of the Namche Barwa Syntaxis, eastern Himalaya: Constraints from deformation, fabrics and geochronology. *Gondwana Res* 21(1): 19-36. <https://doi.org/10.1016/j.gr.2011.06.010>
- Yang D, Chen XQ, Huang Y, et al. (2020) Study on the development characteristics and formation mechanism of the Jiao Bunong Giant Ancient Landslide in Yajiang Suture Zone. *Railway Stand Des* 65(3): 1-9 (In Chinese). <https://doi.org/10.13238/j.issn.1004-2954.202004160002>
- Ye HL, Zheng Y, Li A, et al. (2012) Shaking table tests on stabilizing piles of slopes under earthquakes. *Chin J Geotech Eng* 34(2): 251-257 (In Chinese).
- Yin YP, Wang M, Li B, et al. (2012) Dynamic response characteristics of Daguangbao landslide triggered by Wenchuan earthquake. *Chin J Rock Mech Eng* 31(10): 1969-1982 (In Chinese). <https://doi.org/10.3969/j.issn.1000-6915.2012.10.003>
- Zhang J, Ji J, Zhong D, et al. (2004). Structural pattern of eastern Himalayan syntaxis in Namjagbarwa and its formation process. *Sci China Ser D: Earth Sci* 47(2): 138-150. <https://doi.org/10.1360/o2ydo042>
- Zhang Y, Guo C, Lan H, et al. (2015) Reactivation mechanism of ancient giant landslides in the tectonically active zone: a case study in Southwest China. *Environ Earth Sci* 74(2): 1719-1729. <https://doi.org/10.1007/s12665-015-4180-6>
- Zhang Z, Wang T, Wu S, et al. (2016) Rock toppling failure mode influenced by local response to earthquakes. *B Eng Geol Environ* 75(4): 1361-1375. <https://doi.org/10.1007/s10064-015-0806-x>
- Zhou J, Cui P, Hao M (2016) Comprehensive analyses of the initiation and entrainment processes of the 2000 Yigong catastrophic landslide in Tibet, China. *Landslides* 13(1): 39-54. <https://doi.org/10.1007/s10346-014-0553-2>
- Zhou J, Cui P, Yang X (2013) Dynamic process analysis for the initiation and movement of the Donghekou landslide-debris flow triggered by the Wenchuan earthquake. *J Asian Earth Sci* 76: 70-84. <https://doi.org/10.1016/j.jseaeas.2013.08.007>
- Zhu Y, Dai F, Yao X, et al. (2019) Field investigation and numerical simulation of the seismic triggering mechanism of the Tahman landslide in eastern Pamir, Northwest China. *B Eng Geol Environ* 78(8): 5795-5809. <https://doi.org/10.1007/s10064-019-01541-y>
- Zou Z, Lei D, Jiang G, et al. (2020) Experimental study of bridge foundation reinforced with front and back rows of anti-slide piles on gravel soil slope under El Centro waves. *Appl Sci* 10(9): 3108. <https://doi.org/10.3390/app10093108>